ASTRO-E2 MEMO #2004-03

Title: Characteristics of BI CCD

Category: XIS

Author: Mark Bautz (MIT)

Date: 2004-03-10

Massachusetts Institute of Technology

Center for Space Research
Cambridge, MA 02139
Room 37-521
mwb@space.mit.edu

February 13, 2004
Revised March 10, 2004

To: XIS Team
From: Mark Bautz, Steve Kissel, Beverly LaMarr & Gregory Prigozhin
Subject: Back-illuminated CCDs for Astro-E2 XIS?

1 Summary

This memo summarizes our recent work testing back-illuminated (BI) CCDs for possible use in the XIS. We present measurements of quantum efficiency, spectral resolution, dark current & cosmetic quality, proton radiation tolerance and background rejection efficiency for flight-like and flight-candidate BI devices, and compare them to front-illuminated (FI) devices. Generally, we find that the BI devices meet the expectations raised by the initial results we presented last November. In particular, the BI devices offer quantum efficiency about 3× higher than the FI devices at 525 eV and spectral resolution comparable to that of the FI devices at all energies (BI FWHM within $\sim 15\%$ of FI FWHM.) The BI devices have somewhat thinner depletion regions, leading to lower quantum efficiency in the BI devices at high energies (e.g., by factors of ~ 0.75 and ~ 0.65 at 6.7 and 10 keV, respectively). The BI and FI devices have similar cosmetic quality. While the BI devices show somewhat higher dark current than the FI devices, at the XIS CCD operating temperature (-90C) the BI dark current has no effect on performance. The BI device appears to be slightly more sensitive to proton radiation than the FI CCD, but the charge injection function appears equally effective in suppressing radiation damage effects in the two kinds of sensor. The background rejection efficiency of the BI devices is comparable to that of the FI devices at energies below 1 keV, though, as on ACIS, the rejection efficiency is lower for the BI than the FI at higher energies.

To date we have found no indication (after 400-500 total operating hours with 4 detectors, with more than 24 thermal cycles on one detector) for any temporal instability in the BI device gain or quantum efficiency. We have completed a calibration of one flight-candidate device at MIT, and find that its quantum efficiency can be explained with a simple and physically reasonable model.

The optimum clock voltages for BI and FI devices differ, but both are well within the range available from the XIS AE/TCE.

2 Overview

At the 2003 November XIS team meeting at ISAS, we reported that we had obtained promising initial results with a back-illuminated version of the XIS (MIT/Lincoln Laboratory CCID41) CCD detectors. The device we tested was produced using a so-called chemisorption backside treatment

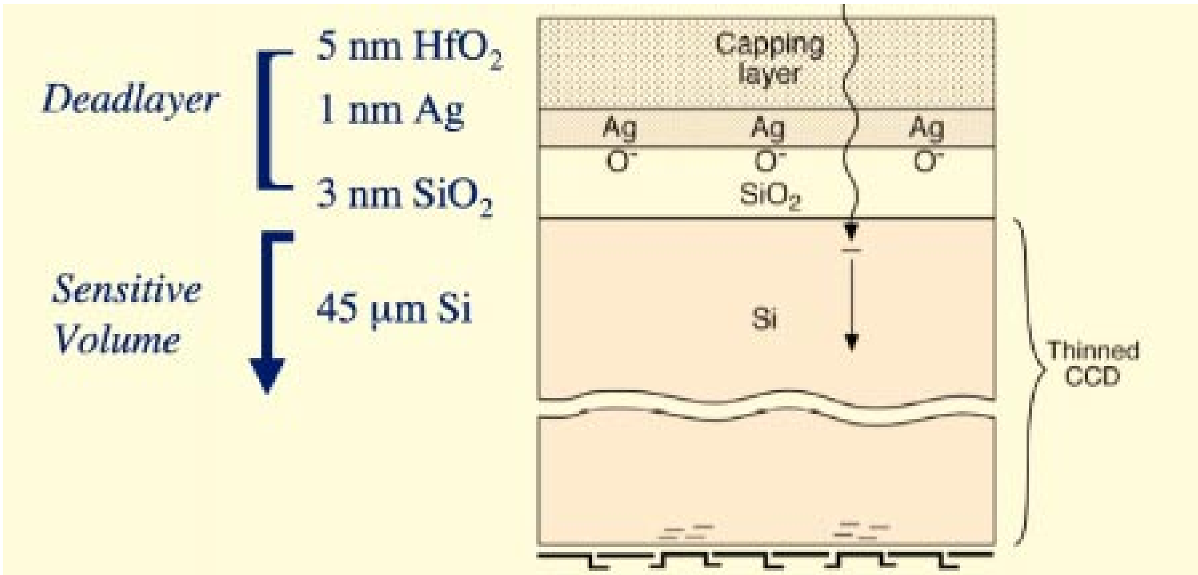

Figure 1: Schematic of back-surface of a back-illuminated detector treated with the chemisorption process. From Lesser et al., 2004.

process developed by M. Lesser at the University of Arizona [Lesser et al. 2004]. Since then we have tested and/or calibrated four BI devices from two different wafers. We report our results here.

In the next section we briefly describe the structure produced by the chemisorption backside treatment process; subsequent sections describe quantum efficiency & spectral resolution, cosmetics, dark current, radiation sensitivity and background rejection efficiency. The final sections summarize our total test time with these detectors and outline differences in detector operating- and event detection-parameters for FI and BI devices.

3 Backside structure produced by the chemisorption charging process

The backside structure is shown schematically in Figure 1 from [Lesser et al. 2004]. The process begins with a thinned wafer on which CCDs have already been fabricated. In our case, the wafers are thinned, nominally, to 45μm. In the chemisorption charging process, the back surface of the thinned wafer is first oxidized. The resulting 3 nm-thick oxide layer is then coated with a very thin ($\sim$ 1 nm) layer of silver; the silver is then capped with a 5nm layer of hafnium oxide. According to [Lesser et al. 2004], the silver catalyzes dissociation of molecular oxygen on the surface during processing, leaving fixed, negatively charged oxygen atoms on the surface. These ions improve the collection of photo-electrons deposited near the back surface. Note that the gate structure of a front-illuminated CCD presents a deadlayer $\sim$ 500 nm thick, so the chemisorption charging process offers, in principle, a factor of $\sim$ 50 reduction in deadlayer thickness.

4 Measured Quantum Efficiency

Measured, spatially-averaged X-ray quantum detection efficiency (QE) for device w1.11c6 is shown in Figure 2. The points were obtained using the standard CSR calibration procedure. The absolute quantum efficiency was measured with respect to a (front-illuminated) reference CCD detector

Material	Thickness
Deadlayer Thicknesses:	
SiO_2	< 18 nm
HfO_2	< 3 nm
Si	70 ± 23 nm
Sensitive layer thickness:	
Si	$37.6 \pm 1.5 \mu$m

Table 1: Best-fit QE model parameter values for BI device w1.11c6. Upper limits and error ranges are at 90% confidence for a single parameter.

that has been calibrated at the PTB beamline at the BESSY synchrotron. Random errors due to counting statistics are negligible; systematic errors are probably about 5% of the measured quantum efficiency at all energies above 277 eV. At 277 eV, the quantum efficiency of the reference detector is not so well known, and we've assumed an error in the measured BI device QE of 25% in fitting the model. For reference, typical FI device QE is shown as the dotted curve in Figure 2.

The BI quantum efficiency measurements shown in Figure 2 have not been corrected for pileup, which may be significant at the lowest energies, so the actual QE of the device may be somewhat higher than is shown in the figure at energies below 1 keV.

We fit deadlayer models containing the components shown in Figure 1, multiplied by an overall scale factor and by an effective deadlayer of silicon to represent charge losses near the back surface. We also allowed the overall thickness of the device (nominally 45μm) to be a free parameter in the model. The best-fit model, shown as the solid line in Figure 2, has parameter values listed in Table 1.

Three features of the best-fit model are particularly interesting. First, the very thin silicon dioxide and hafnium oxide layers evidently have little effect on the device quantum efficiency; the best-fit thicknesses for these layers are consistent with 0. Second, the model contains an apparent deadlayer of silicon which, at ~ 70nm is considerably thicker than the oxide layers, though much thinner than the deadlayer of a front-illuminated CCD (~ 550 nm). Finally, the apparent thickness of the device is about 38 μm, which is less than the thickness of the depletion region in XIS front-illuminated devices ($60 - 65 \mu$m.) As a result, the quantum efficiency of the BI devices is less than that of an FI device at energies E$>$ 4.5 keV or so.

Finally, we compare the overall effective area of a single FI vs. a single BI XIS sensor in Figure 3. Here we have included the XRT-I effective area and thermal shield (courtesy of Ishida-san) and the XIS optical blocking filter (courtesy of Kitamoto-san.) This figure shows that the fractional increases in effective area below 2 keV are generally much larger than the fractional loss of effective area at high energies. Note that the BI CCD provides significant collecting area below the carbon K-edge at 284 eV.

5 Spectral Resolution

The spectral resolution of BI and FI XIS devices is compared in Figure 4. The back-illuminated CCDs we are considering for the XIS have spectral resolution quite comparable to that of FI devices. In this regard they are quite different from all previous generations of back-illuminated X-ray CCD devices, including those used on *Chandra* and *XMM/Newton*, which have spectral resolution roughly a factor of two worse than similar FI devices.

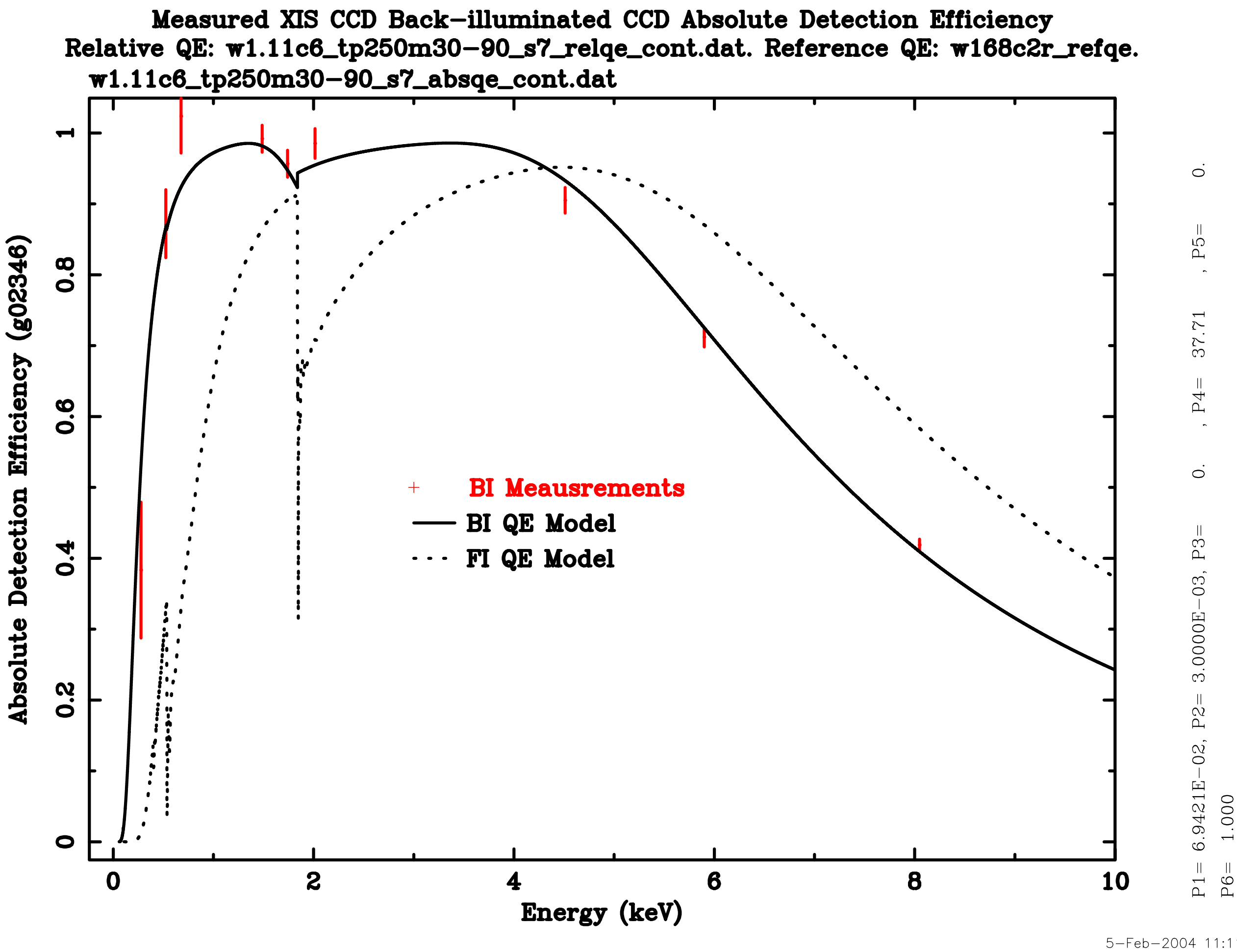

Figure 2: Measured absolute quantum efficiency (points) and best-fit quantum efficiency model (solid line) for back-illuminated device w1.11c6. The best-fit measured QE of front-illuminated XIS device w1.3c6 is shown as the dotted curve.

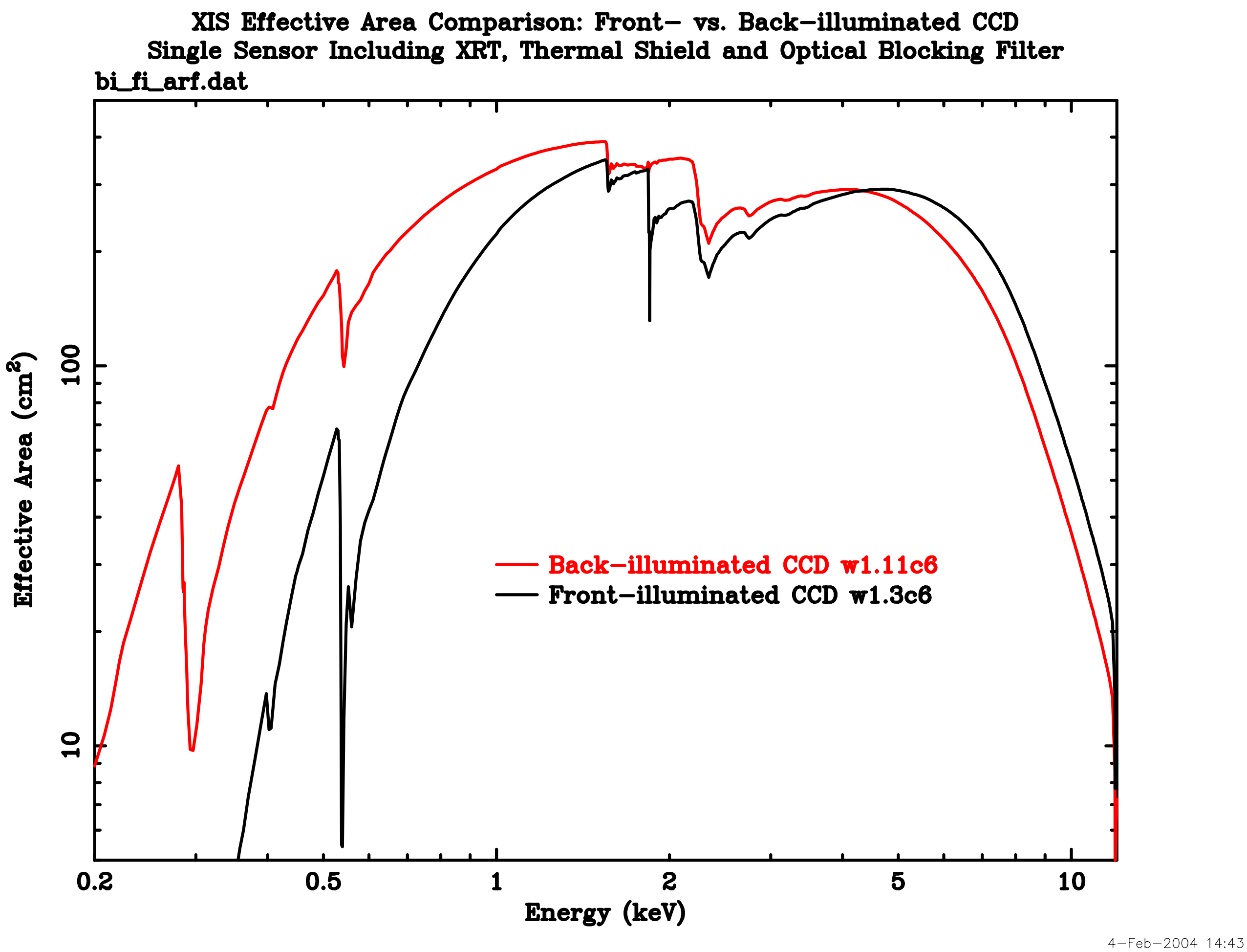

Figure 3: Comparison of effective area, for one XIS sensor, for BI (red) and FI(black) CCDs. Note that logarithmic axes are used. The XRT-I effective area, XRT thermal shield transmission, and XIS optical blocking filter transmission are included in the calculation. The CCD efficiencies are best-fit models to measurements of w1.11c6 (BI) and w1.3c6(FI), respectively.

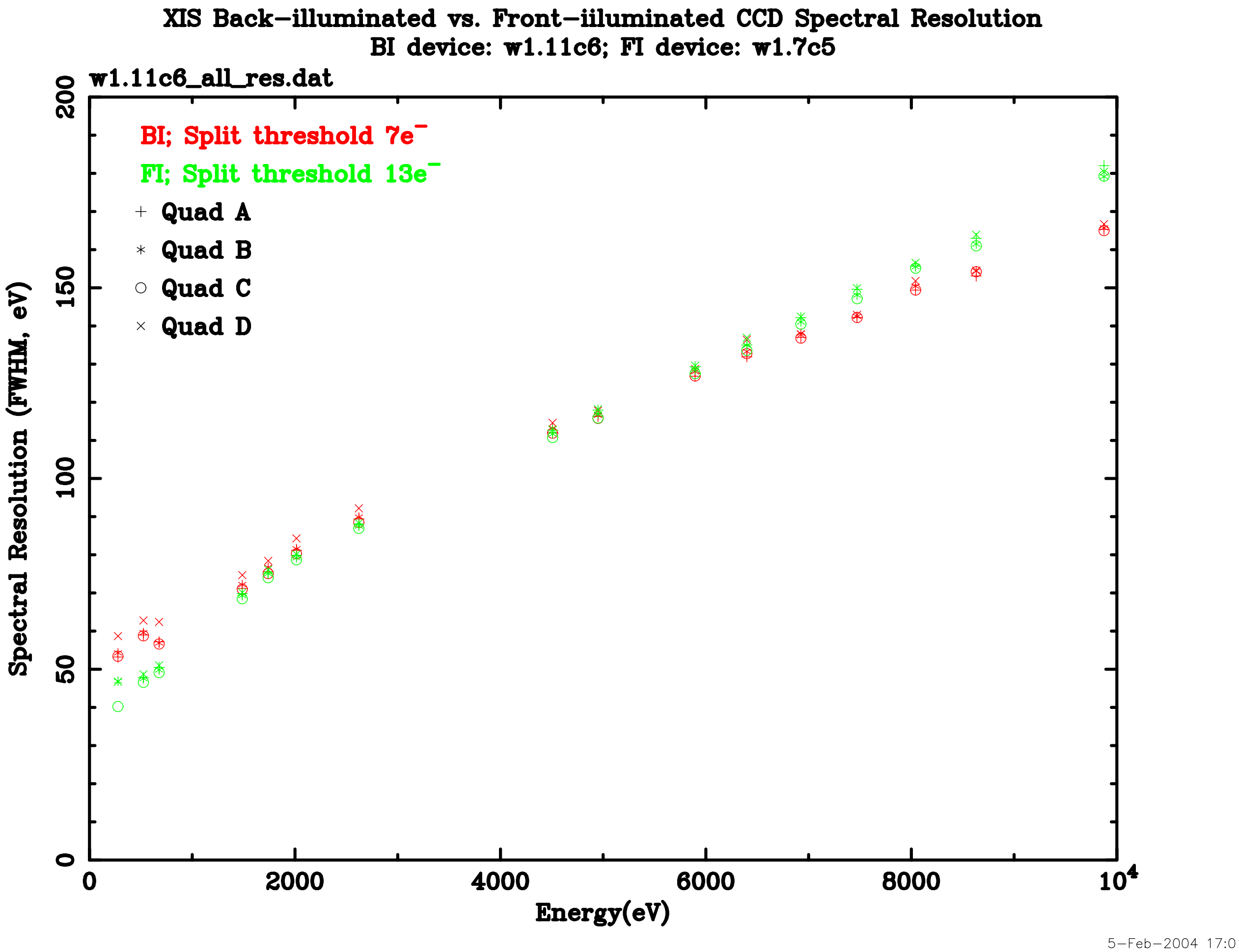

Figure 4: Comparison of spectral resolution (FWHM in eV) for back-illuminated (red points) and front-illuminated (green points) XIS devices. The optimum split event thresholds are different for the two device types. Data are from BI device w1.11c6 and FI device w1.7c5.

Figure 4 shows that the XIS BI devices have spectral resolution that is comparable to, though somewhat worse (FWHM $\sim 15-20\%$ greater) than the FI devices at the lowest energies. The BI devices actually have slightly better spectral resolution at the highest energies. Note that, for the BI devices, a split threshold of $7e^-$ seems to provide the best compromise between quantum efficiency and spectral resolution at low energies. (All BI quantum efficiencies reported were obtained with a split threshold of $7e^-$). The BI split threshold is thus considerably lower than the $13e^-$ value used for FI devices.

To compare the scientific quality of spectra produced by the two device types, we show in Figure 5 simulated spectra for the supernova remnant E0102-72.3. In each case the count rates pertain to a single XIS sensor. A very long exposure (10^5 s) to this bright source was simulated to illustrate the response differences between the BI and FI devices. The spectral model is based on the Chandra HETG spectrum of this source ([Flanagan et al., 2004]). The simulations show that the same spectral features are clearly resolvable by both devices, and that the BI devices provide a factor of 3-4 higher counting rate at the O VIII Lyman α (0.66 keV) and OVII triplet (0.57 keV), respectively. Integrated over the 0.2-2.5 keV band, the BI counting rate is a factor of two greater than the FI counting rate for this source.

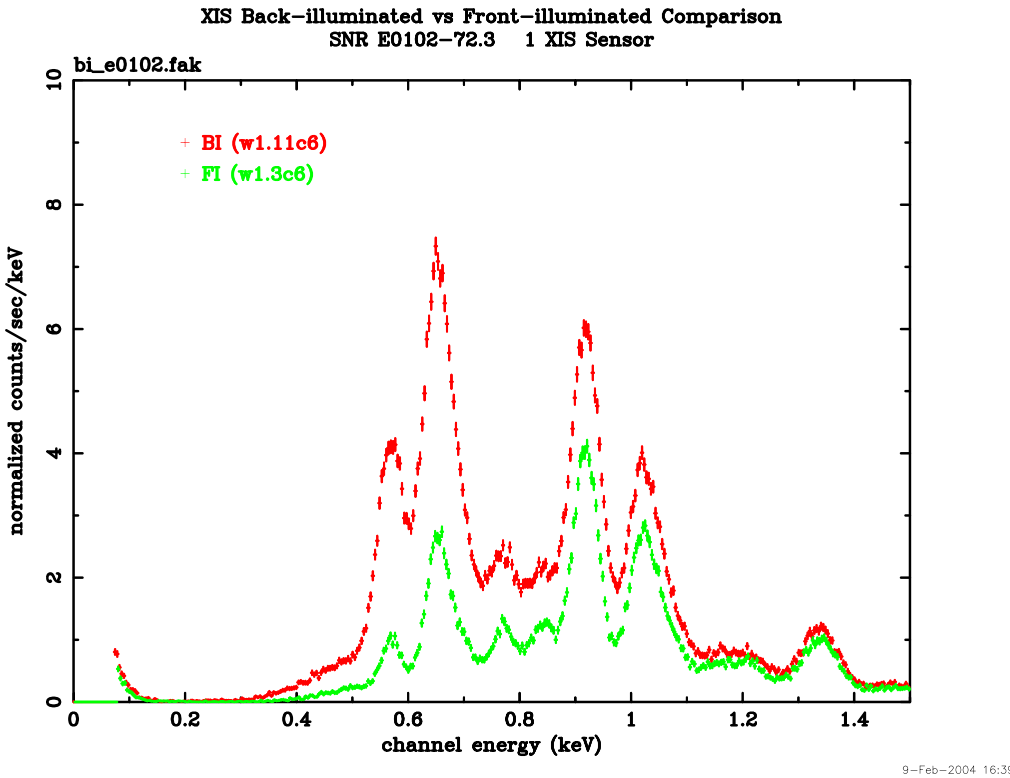

Figure 5: Simulated spectra of the SNR E0102-72.3 for BI (red) and FI (green) devices. In each case the counting rates are for a single sensor. The same spectral features are visible with both device types but the BI device provides a counting rate higher by as much as a factor of 4 (at the OVIII triplet at 0.57 keV.) The broadband (0.2-2.5 keV) counting rate is higher for the BI device by a factor of 2.

For comparison to current-generation BI CCDs, we show in Figure 6 the simulated XIS spectra of E0102-72.3 (repeated from Figure 5) as well as simulations (obtained with the same spectral model) of *Chandra* ACIS-S and *XMM/Newton* EPIC-PN observations of this source. The XIS BI device provides much higher spectral resolution than either of these two other instruments. (Note that EPIC-MOS spectral resolution is comparable to that of both FI and BI XIS devices; strictly speaking, EPIC MOS CCDs are not back-illuminated.) For this source, a single XIS BI sensor is roughly equivalent in effective area two XIS-FI sensors, or one *XMM-Newton*/EPIC-MOS camera, o r about 75% of *Chandra* ACIS-S. Two XIS-BI sensors alone would provide about 50% higher counting rate (for this source) than ACIS-S, but with much better (low-energy) spectral resolution than either ACIS-S or EPIC-PN.

6 Dark Current and Cosmetics

The mean (spatially averaged) dark current of BI and FI devices is shown as a function of temperature in Figure 7. The BI devices have uniformly higher dark current. At a nominal operating temperature of -90C, and a frame time of 8s, however, mean dark current will be less than 1 e^- $pixel^{-1}$ per frame, and so is negligible from a performance point of view.

Statistics of hot pixels and bad columns are compared for a number of devices in Table 2. Hot pixels have exceptionally high dark current, and are defined for purposes of this table as pixels

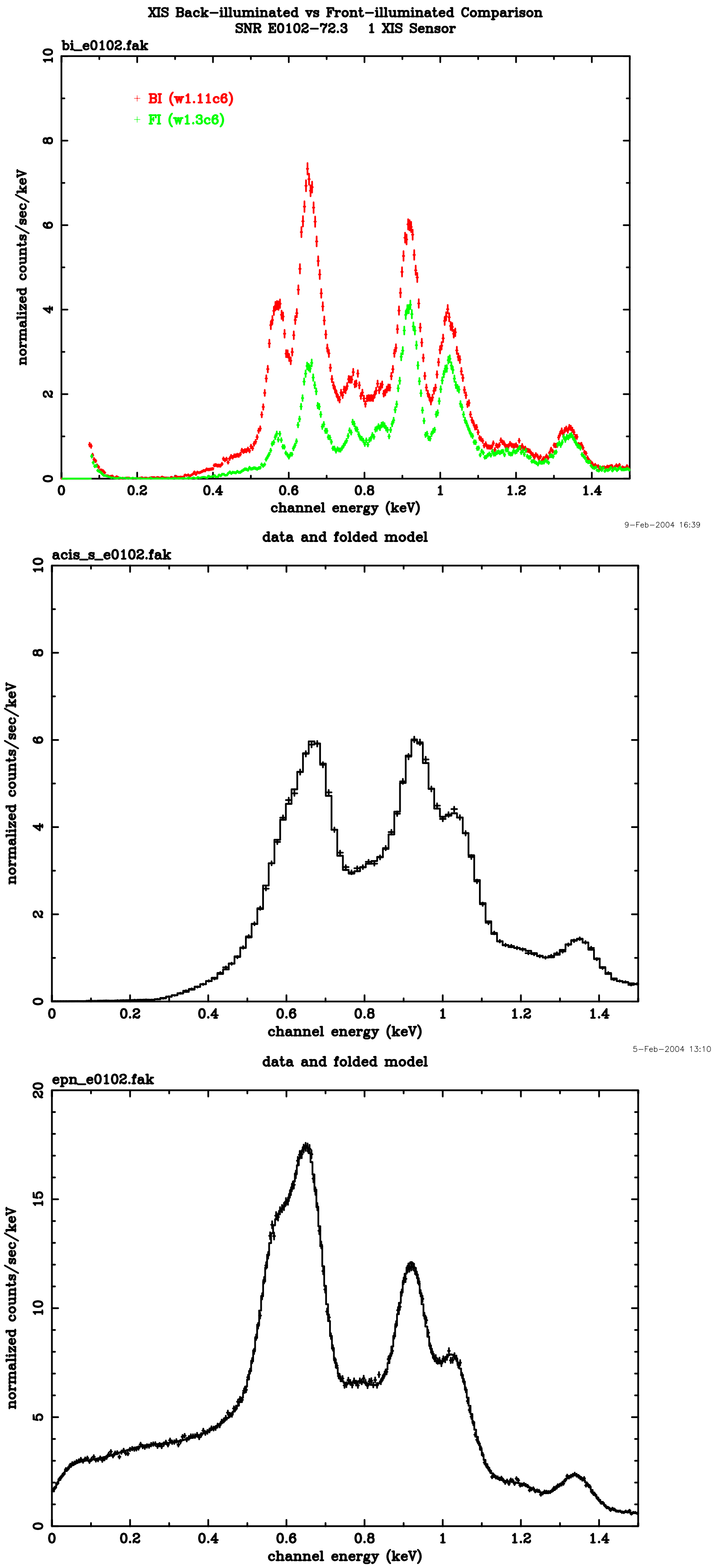

Figure 6: Simulated spectra of the SNR E0102-72.3[8] for XIS *(top)* ACIS-S *(middle)* and EPIC-PN *(bottom)* using a spectral model derived from Chandra grating data. The top panel shows both BI (red) and FI (green) spectra for one XIS sensor, repeated from the previous figure. One XIS BI sensor provides effective area nearly equivalent to one XMM EPIC-MOS camera; two would provide about 50% more effective area than ACIS-S.(NB: Vertical scales differ.)

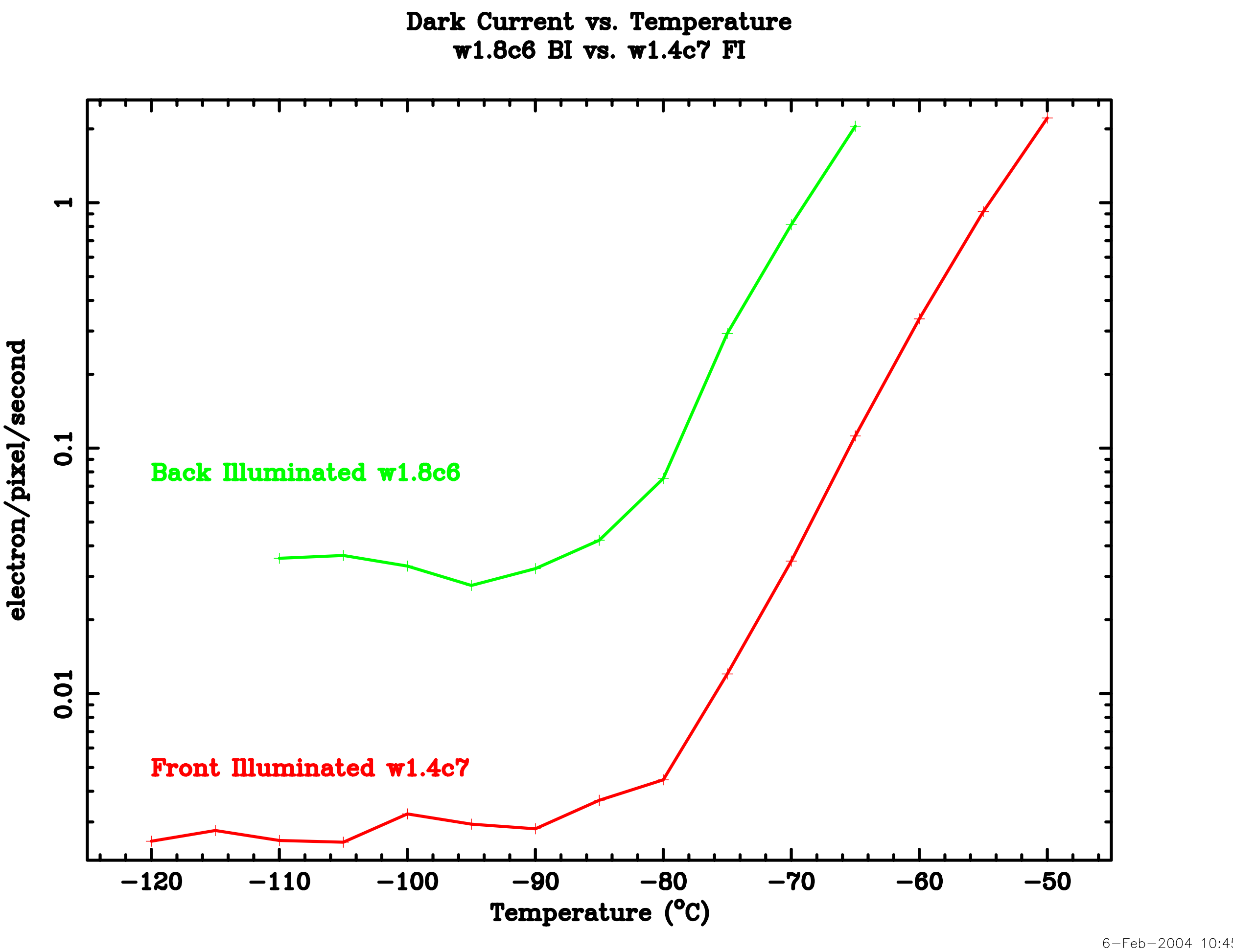

Figure 7: Comparison of dark current measured for back-illuminated (red points) and front-illuminated (green points) XIS devices. At the nominal frame time of 8s or less, and the nominal operating temperature of -90C, dark current will be negligible for both device types.

Device	FI/BI	Hot Pixels		Bad Columns	Remarks
		Total	Isolated		
w1.14c8	FI	48	48	TBD	Flight spare
w1.14c7	FI	18	18	34	
w1.3c6	FI	54	30	27	24 hot pixels in worst column
w1.7c6	FI	45	45	36	
w1.7c5	FI	31	31	24	
w1.11c6	BI	635	39	TBD	596 hot pixels in 2 worst columns
w1.8c6	BI	1020	24	TBD	996 hot pixels in 2 worst columns
w1.8c5	BI	31	31	18	Flight candidate

Table 2: Hot pixel and defective column counts for the XIS flight FI devices and for several BI devices. "Isolated" hot pixels are those remaining after one or two columns containing more than 10 hot pixels each are excluded.

that show an anomalously high event rate (more than 10 standard deviations above the mean) during X-ray calibration Although the total number of hot pixels seems to be higher in the BI devices, most of these are concentrated in one or two defective columns. If these defective columns are excluded, then the number of hot pixels is comparable in the BI and FI devices. It should be noted that the effect of hot pixels depends on the method for dark level determination. The XIS DE provides for pixel-by-pixel dark level determination, so hot pixels can effectively be vetoed by on-board processing.

A bad column is one in which at least 10% of the column is blocked and so effectively photo-insensitive. Bad columns are identified from very long ($\sim 10^7$-event) exposures to an X-ray calibration source. The BI and FI devices have similar numbers of bad columns.

7 Radiation Tolerance

We have irradiated one front-illuminated and one back-illuminated XIS CCD with 40-MeV protons. The experiments were done at the Northeast Proton Therapy Center affiliated with the Massachusetts General Hospital. In these tests, 235-MeV protons produced in a cyclotron pass through a plastic degrader, emerging with an energy of 40 MeV ($\pm$ roughly 5 MeV). The proton beam is then "collimated" by a $\sim$ 1 cm-diameter circular aperture in a $\sim$ 5 cm-thick lead shield before striking the CCD. Thus only a portion of the (2.5 cm $\times$ 2.5 cm) CCD is actually irradiated. Devices are irradiated at room temperature with all leads shorted. For each device the total fluence ($2.0 \pm 0.2 \times 10^9$ protons cm^{-2}) is delivered in a period of 1 minute or so. We estimate that this dose is equivalent to roughly 2 years exposure to on-orbit proton irradiation.

Protons of this energy increase dark current and charge transfer efficiency (CTI.) The change in CTI manifests itself in decreasing pulse-height ("gain") and declining spectral resolution with increasing row number. Plots of the center-pixel pulse-height vs. row relationship both before and after irradiation, for both BI and FI devices are shown in Figure 8. These curves were obtained by illuminating the irradiated device with X-rays from a radioactive ^{55}Fe source; the detector temperature was -90C during the CTI measurements. The slope of the pulse-height vs. row characteristic is proportional to the CTI. The change in this slope, measured in the irradiated portion of the CCD, gives the change in CTI due to the proton irradiation. Corresponding changes

Device	FI/BI	CTI Change due to Irradiation	
		Without Charge Injection	With Charge Injection
w1.8c6	BI	8.8 ± 0.7	1.6 ± 0.7
w1.6c1	FI	5.7 ± 0.2	0.4 ± 0.3

Table 3: Change in CTI (in units of 10^{-5} per pixel measured at 5.9 keV) due to irradiation by 40 MeV protons (nominal fluence 2.0×10^9 protons cm^{-2}, roughly equivalent to 2 years of on-orbit exposure) for the XIS BI and FI devices. Values obtained with and without charge injection are listed.

in spectral resolution (FWHM at 5.9 keV) are shown in Figure 9.

The nominal CTI changes (at 5.9 keV) due to the proton irradiation are compared in Table 3. The BI device appears to have experienced a somewhat larger change in CTI than the FI device, by a factor of 1.5 ± 0.15. It is not clear why this is so. Three possibly contributing factors may be i) The modest increase in linear energy transfer (dE/dx) of the incident protons as a result of traversing the $\sim 40\mu$m thick silicon in the BI device before reaching the buried channel. This effect might be expected to increase the BI radiation sensitivity we measure by about 10%, relative to the FI devices; ii) the different clock voltages used for the two types of device; and iii) the smaller sacrificial charge effect in the BI devices due to the absence of undepleted silicon. We note that when charge injection is employed, the radiation sensitivity of both device types is significantly reduced, and in fact is formally indistinguishable with these data.

8 Background Rejection Efficiency

In order to check the relative background rejection efficiencies of the FI and BI devices, one CCD of each type was illuminated by a ^{60}Co source. The gammas and secondary electrons from this source mimic, to some extent, the charged particle background encountered on-orbit. Standard X-ray event selection criteria were applied, but for reasons described above in the discussion of spectral resolution, the BI data were processed using a split-event threshold of 7 adu (roughly 1 adu $\sim$ 1 e^-) while a split threshold of 13 adu was used for the FI data. The resulting residual background spectra are compared in Figure 10.

Figure 10 shows that, at energies below about 1.5 keV, the residual background (and hence the charged particle background rejection efficiency) is about the same for the two detector types. In the vicinity of the the silicon K fluorescence line at 1.74 keV, the BI rejection efficiency is much better than the FI; integrated over the 1-2.5 keV, the BI rejection efficiency is better by a factor of roughly 2. At higher energies, the FI rejection efficiency gets better relative to the BI. Integrated over the 2.5 - 12 keV band, the FI rejection efficiency is better by a factor of about 2.5. The large undepleted bulk of the FI devices evidently enhances the rejection efficiency for high-energy particles, although it also apparently causes a brighter silicon fluorescence line.

9 Operating Experience

9.1 Test time summary

We have tested 4 BI devices to date, two each from two wafers. A third wafer is in process at this writing. Wafer 11 devices were (intentionally) fabricated without charge injection. Wafer 8 devices have charge injection.

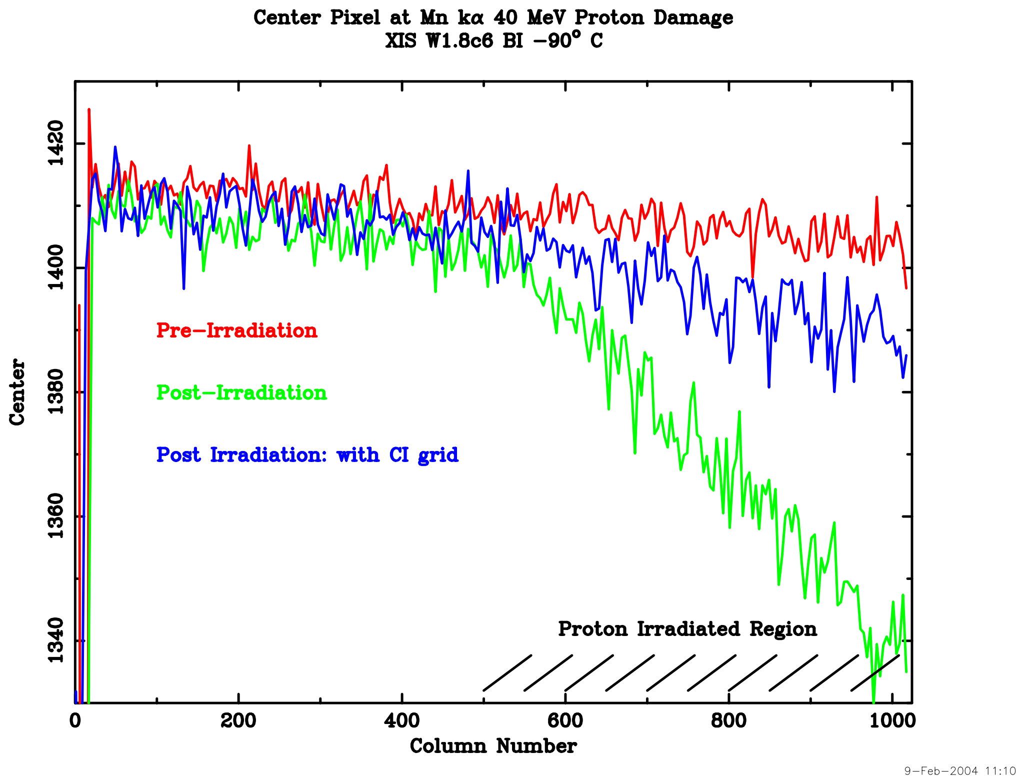

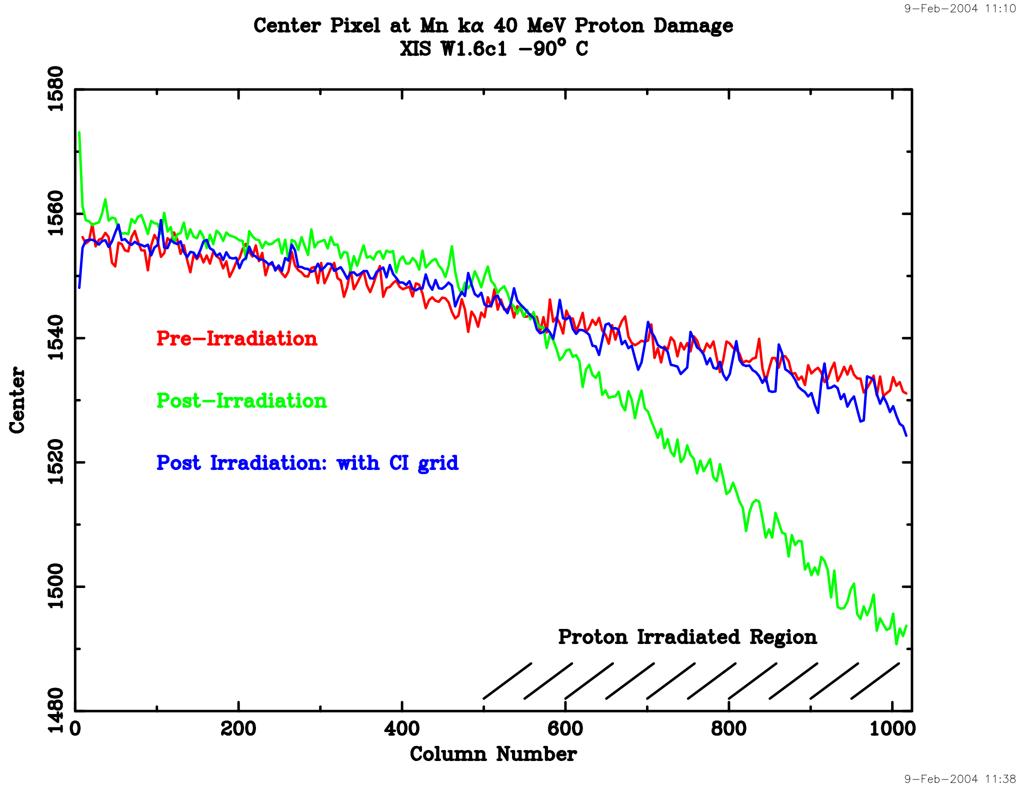

Figure 8: Center-pixel pulse-height of 5.9 keV X-ray events vs CCD row number for BI (top) and FI(bottom) devices irradiated with $2.0 \pm 0.2 \times 10^9$ p cm^{-2} of 40 MeV protons. Pre-irradiation data are shown for comparison, and the effect of including charge-injection after the irradiated side is also shown.

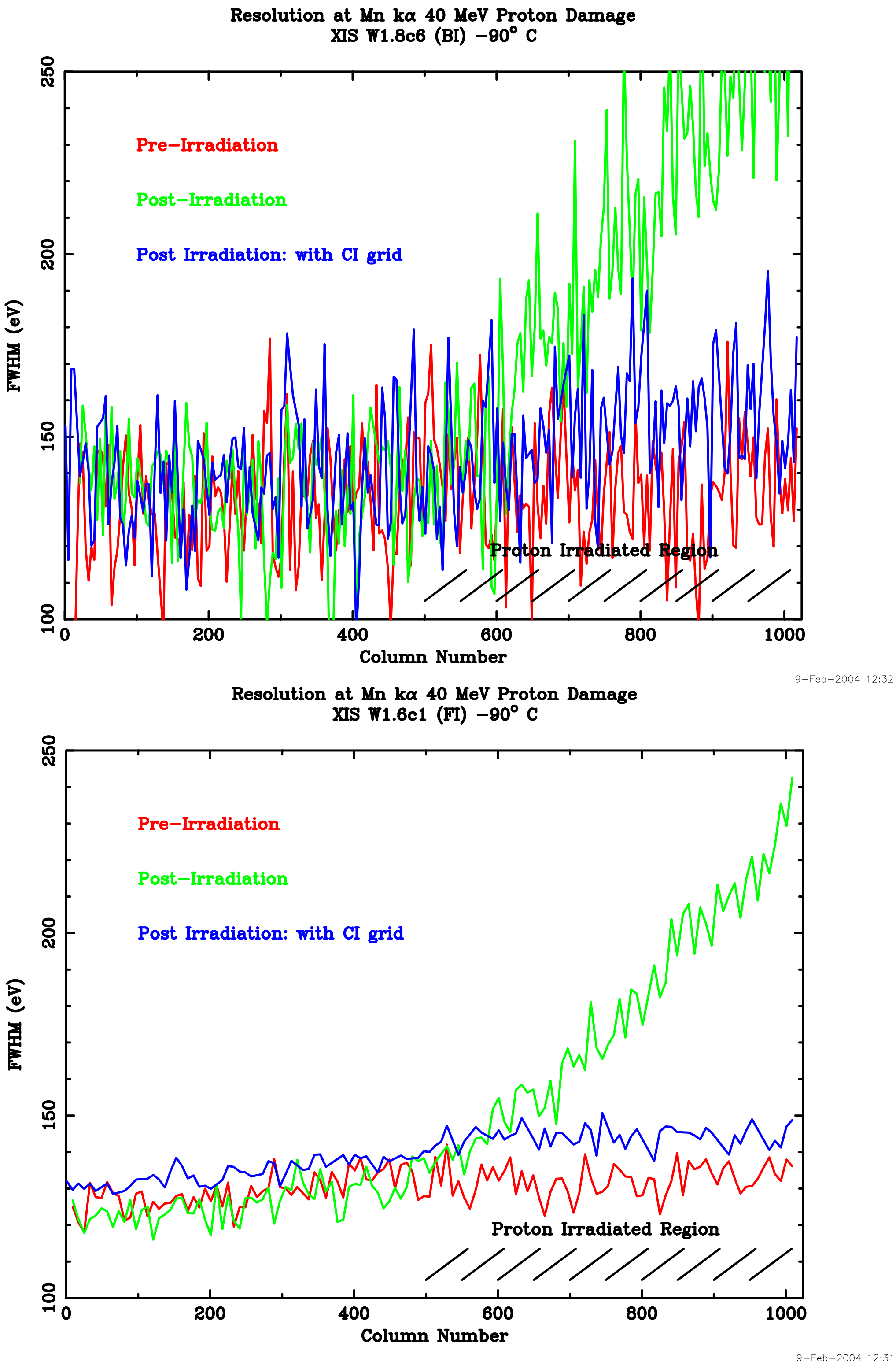

Figure 9: Spectral resolution (FWHM)of 5.9 keV X-ray events vs CCD row number for BI (top) and FI(bottom) devices irradiated with $2.0 \pm 0.2 \times 10^9$ p cm^{-2} of 40 MeV protons. Pre-irradiation data are shown for comparison, and the effect of including charge-injection after the irradiation is also shown.

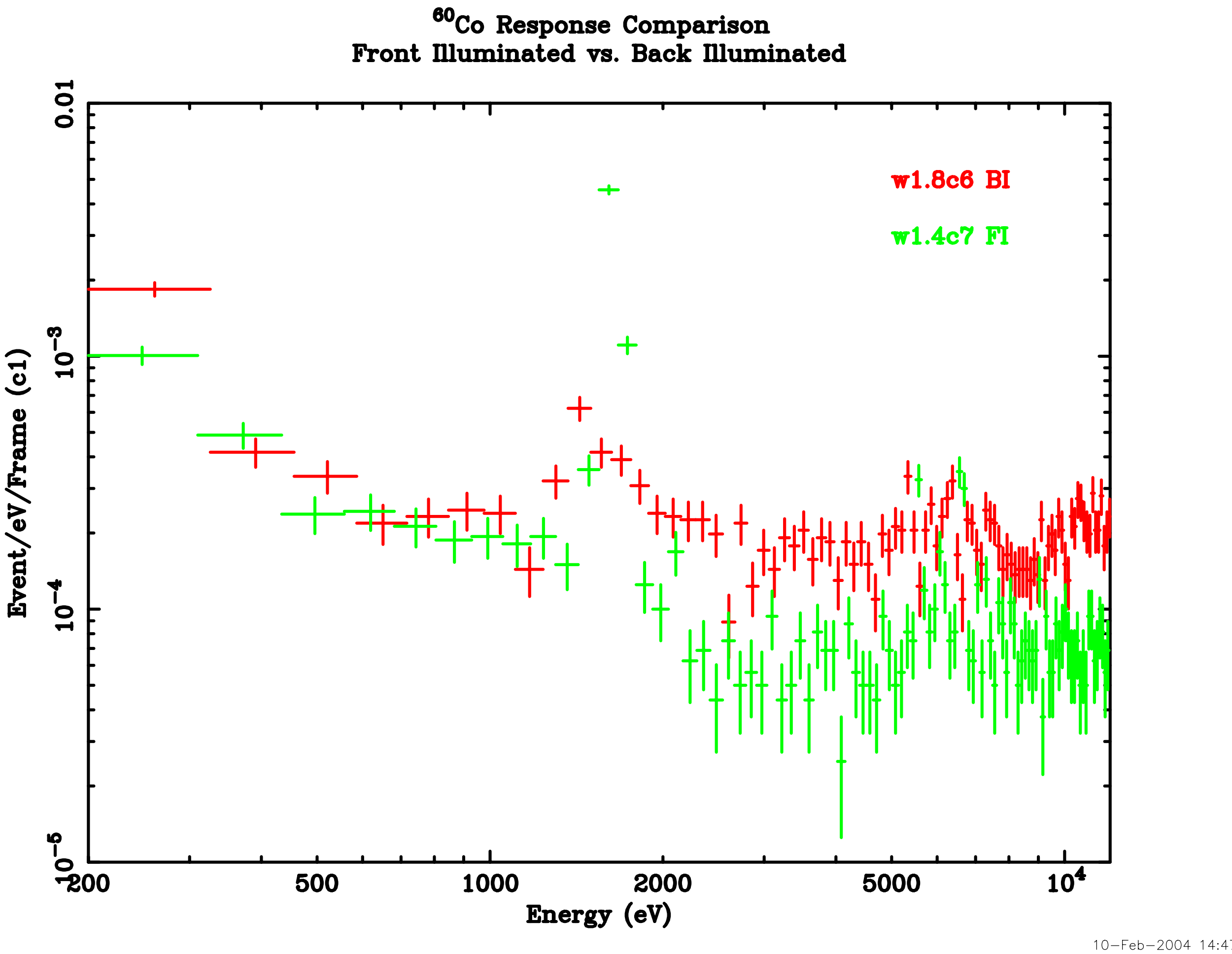

Figure 10: Residual background spectra produced by a ^{60}Co source in BI (red) and FI (green) CCDs. At energies below about 1.5 keV, the residual background (and hence the charged particle background rejection efficiency) is about the same for the two detector types. At higher energies, the FI rejection efficiency is better by a factor of about 3.

We have subjected one device (w1.8c5) to a complete calibration (very roughly 200 hours of operation over a three-week period. We believe this device is of flight quality and we expect to install it in a flight sensor base during the month of February.

We have accumulated a total of approximately 300 hours of test time on the other three devices over a four month period. One of these devices (w1.11c6) has received a nearly complete calibration and is not presently regarded as a flight candidate only because it is not equipped with charge injection. Another device (w1.8c6) has been subjected to at least 24 thermal cycles; this same device has been irradiated with 40 MeV protons. Once the proper operating point for the BI devices was established (see below), we found no evidence for peculiar or unstable behavior. We are continuing testing to check stability.

We expect delivery of additional BI devices (from the third wafer to be treated with the chemisorption charging process) within the month.

9.2 Differences between FI and BI device operating points.

Currently the FI uses +7 -6 volt serial clocks (dacs=140, 120). These values have propagated from the original Astro-E design. While there is some evidence that they may not be optimal these values provide good performance in the FI devices. For the (4) BI devices we have found that these levels are inappropriate since they produce noise in excess of 20e per readout. Instead, values of +4.5 -4.5 volt (dacs=90, 90) are used for the serial clocks. Further reduction of serial clock level complicates the charge injection operation and does not improve performance.

The current BI devices do not work well if the image clock level moves into inversion. For this reason we use +12 -2.5 volts for the image clock and for convenience have removed the SEQI commands from the sequencer. The SEQI commands could be restored if power consumption during parallel transfer becomes an issue. A consequence of these image clock voltages is that a one-time "jitter dacs" step is required each time the CCD is power is turned on . (Such a step is routinely used in ACIS operations.) As expected, the BI produces more split events at all energies than does the FI. Consequently the importance of the previous noise-reduction steps is magnified since more pixels are used per event. Also, the split threshold for the BI needs to be lower to recover event charge.

References

[Lesser et al. 2004] Burke, B., Lesser, M. et al. 2004 IEEE Nuclear Science Symposium (submitted).

[Flanagan et al., 2004] Flanagan, K.A., Canizares, C. R., Dewey, D., Houck, J. C., Fredericks, A. C., Schattenburg, M. L., Markert, T. H. & Davis, D. S., 2004, ApJ, (in press). (astro-ph/0312509)